Geophysical Research Letters

RESEARCH LETTER
10.1029/2021GL092609

Persistent Stratospheric Warming Due to 2019–2020 Australian Wildfire Smoke

Pengfei Yu[1], Sean M. Davis[4], Owen B. Toon[2,3], Robert W. Portmann[4], Charles G. Bardeen[5], John E. Barnes[6], Hagen Telg[6], Christopher Maloney[7,4], and Karen H. Rosenlof[4]

[1]Institute for Environmental and Climate Research, Jinan University, Guangzhou, China, [2]Laboratory for Atmospheric and Space Physics, University of Colorado, Boulder, CO, USA, [3]Department of Atmospheric and Oceanic Sciences, University of Colorado, Boulder, CO, USA, [4]Chemical Science Laboratory, National Oceanic and Atmospheric Administration, Boulder, CO, USA, [5]Atmospheric Chemistry Observations and Modeling, National Center for Atmospheric Research, Boulder, CO, USA, [6]Global Monitoring Laboratory, National Oceanic and Atmospheric Administration, Boulder, CO, USA, [7]Cooperative Institute for Research in Environmental Sciences, University of Colorado, Boulder, CO, USA

Key Points:

- The 2019–2020 Australian wildfire injected about 0.9 Tg smoke containing 2.5% black carbon into the stratosphere
- Climate model simulations indicate that the smoke warmed the Southern Hemisphere stratosphere by 1 K for more than 6 months
- Model calculations estimate a decrease in ozone of 10–20 Dobson units from August to December at mid-high southern latitudes

Supporting Information:

Supporting Information may be found in the online version of this article.

Correspondence to:

P. Yu,
pengfei.yu@colorado.edu

Citation:

Yu, P., Davis, S. M., Toon, O. B., Portmann, R. W., Bardeen, C. G., Barnes, J. E., et al. (2021). Persistent stratospheric warming due to 2019–2020 Australian wildfire smoke. *Geophysical Research Letters*, *48*, e2021GL092609. https://doi.org/10.1029/2021GL092609

Received 25 JAN 2021
Accepted 11 MAR 2021

Abstract Australian wildfires burning from December 2019 to January 2020 injected approximately 0.9 Tg of smoke into the stratosphere; this is the largest amount observed in the satellite era. A comparison of numerical simulations to satellite observations of the plume rise suggests that the smoke mass contained 2.5% black carbon. Model calculations project a 1 K warming in the stratosphere of the Southern Hemisphere midlatitudes for more than 6 months following the injection of black-carbon containing smoke. The 2020 average global mean clear sky effective radiative forcing at top of atmosphere is estimated to be -0.03 W m^{-2} with a surface value of -0.32 W m^{-2}. Assuming that smoke particles coat with sulfuric acid in the stratosphere and have similar heterogeneous reaction rates as sulfate aerosol, we estimate a smoke-induced chemical decrease in total column ozone of 10–20 Dobson units from August to December in mid-high southern latitudes.

Plain Language Summary The 2019–2020 Australian bushfires injected a large amount of smoke that rose well into the stratosphere due to absorption of solar energy. A climate model is used to simulate the plume rise, transport, chemical, and climate impacts of the smoke from these massive bushfires. Simulations suggest that the smoke remained in the stratosphere for all of 2020 and that it measurably warmed the stratosphere by about 1–2 K for more than 6 months. The smoke particles were transported to high latitudes in the Southern Hemisphere and assuming similar heterogeneous reaction rates as sulfate aerosol should have produced about 4%–6% loss of the total column at high southern latitudes.

1. Introduction

The December 29, 2019–January 4, 2020 Australian New Year (ANY) wildfire exceeded the 2009 Black Saturday fires as the most devastating in Australian history. Extreme wildfires can inject smoke into the upper troposphere and even into the stratosphere under favorable meteorological conditions (Fromm et al., 2010). The higher the smoke is injected, the longer it will persist and the wider its extent. The 2017 Pacific Northwest Wildfire Events (PNE) injected about 0.3 Tg of smoke particles into the stratosphere and elevated the stratospheric aerosol extinction above background for over 8 months (Peterson et al., 2018; Yu et al., 2019). The impact from the ANY is expected to be much larger than the 2017 PNE as it injected a greater amount of smoke (Kablick et al., 2020; Khaykin et al., 2020).

Wildfire smoke particles are mainly composed of organic carbon (OC) and black carbon (BC) (Andreae, 2019). OC is largely nonabsorbing at mid-visible wavelengths while BC is a strong visible light absorber. A portion of OC, which is referred to as brown carbon (BrC), can absorb sunlight, but the absorption is much weaker than BC, and observations suggest these aerosols have a lifetime of only a few days (Forrister et al., 2015). When BC absorbs sun light it warms the surrounding air and lofts the heated air parcel (de Laat et al., 2012; Malone et al., 1985; Yu et al., 2019). The degree of heating and ascent of the air parcel scales with the mass fraction of BC. The BC mass fraction depends on the fuel type and the fire characteristics,

but typically BC makes up about 2% of smoke from boreal forest, 3% of that from temperate forest, and as much as 8% of smoke from savanna and grassland fires based on numerous field studies summarized in Andreae (2019). The BC mass fraction was estimated to be 2%–3% in the PNE stratospheric aerosols and in the 2013 California Rim fire boundary layer aerosols (Yu et al., 2016, 2019).

Stratospheric and tropospheric smoke particles significantly perturb the Earth's radiative balance through both shortwave scattering and longwave absorption. A comparison between observations and a numerical forecast lacking fire smoke demonstrated that a 1987 California fire cooled the local surface temperature by 15K (Robock et al., 1988). Modeling studies estimate that a 5-Tg BC injection from a regional nuclear war could warm the global stratosphere by 30 K (Mills et al., 2008), decrease the incoming shortwave flux at the planetary surface by over 10%, and cool the global average surface by about 1.5 K (Toon et al., 2019).

The 2017 PNE smoke was observed to have spread throughout most of the Northern Hemisphere (NH) stratosphere after about 2 months by the SAGE III/ISS, the Ozone Mapping and Profiler Suite Limb Profiler (OMPS-LP) and other satellites instruments (Khaykin et al., 2018; Torres et al., 2020; Yu et al., 2019). Similarly, in the 2019–2020 Australian event, the smoke particles were detected throughout the Southern Hemisphere stratosphere (SHS) after a few months by the spaceborne SAGE III/ISS and OMPS instruments (Kablick et al., 2020; Khaykin et al., 2020). Numerical models suggest that the 2017 PNE smoke, with slightly less than 0.1% of the BC (about 7.5×10^{-3} Tg) as compared a regional nuclear war scenario (Toon et al., 2019), could warm the air parcels up to 6 K locally within the concentrated smoke plume (Yu et al., 2019). However, simulations of 2017 PNE did not show significant temperature anomalies on the hemispheric scale. In this study, we demonstrate that the amount of BC emitted during the 2019–2020 Australian fire could perturb stratospheric temperatures and the radiative balance on a hemispheric scale. That aerosols can warm the stratosphere is not an unprecedented conclusion in that Free and Angell (2002) showed that several volcanic clouds heated the stratosphere by 1 K. However, the injected aerosol mass of these volcanic clouds was an order of magnitude greater than that of the smoke. We also discuss how this record-breaking smoke event might have affected the high-latitude ozone burden, which had near record losses in October of 2020.

2. Methods

We use a sectional aerosol model, the Community Aerosol and Radiation Model for Atmospheres (CARMA) coupled with the Community Earth System Model (CESM-CARMA) (Bardeen et al., 2008; Toon et al., 1988; Yu et al., 2015, 2019) to study the transport, microphysics, chemistry and climate impacts of smoke from the extensive ANY event. The model has 56 vertical layers from the surface up to 45 km with a vertical resolution of about 1 km in the upper troposphere and lower stratosphere, and simulations are run on a grid of 1.9° latitude × 2.5° longitude. Details of the model configuration are in the Supporting Information (Text S1).

Peterson et al. (2020) estimated that the ANY smoke mass injected into the stratosphere was between 0.3 and 0.9 Tg; where 0.9 Tg is three times that of the 2017 PNE smoke estimate (Yu et al., 2019). Khaykin et al. (2020)'s estimate on ANY smoke mass is 0.4±0.2 Tg, which is about 45% of our estimate. In our initial calculations, we increased the PNE smoke particulate emission, 0.3 Tg of smoke, by a factor of 3 for the 2019 Australian fire event simulation (3xPNE). To test the sensitivity to smoke amount, we also examined two other emission scenarios, one with the same emissions as in 2017 (1XPNE) and one with five times the emissions of the 2017 case (5XPNE). Smoke is injected in the upper troposphere at 12 km within one model grid box (modeled local tropopause is 15.5 km) over Southeastern Australia near (39°S,150°E), and we assume the injected BC mass fraction is 2.5%, similar to the values derived from the 2017 PNE (Yu et al., 2019) and 2013 Rim fire (Yu et al., 2016). To test the sensitivity to BC fraction, we performed additional experiments with BC fraction values of 0% and 5%. In the smoke, 20% of OC is co-emitted with BC and the remaining 80% of OC is injected externally mixed. We inject the smoke at a constant rate from 0Z to 5Z UTC (10 a.m. to 3 p.m. local time) on 4 individual days (December 29–31, 2019 and January 4, 2020), corresponding to the dates pyrocumulonimbus were observed reaching the stratosphere (Kablick et al., 2020).

The model is spun up in specified dynamics mode for 6 months until December 29, 2019 by nudging to the Goddard Earth Observing System version 5 analysis (GEOS-5). Starting from December 29, we run two sets

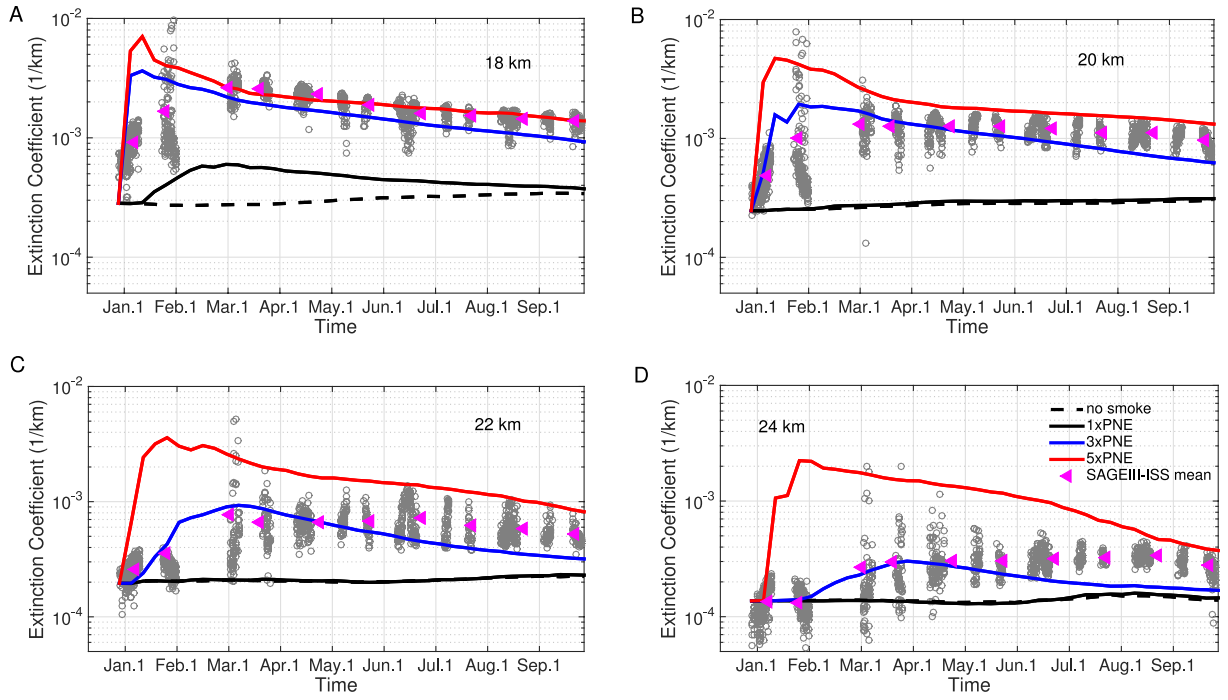

Figure 1. Simulated temporal distribution of aerosol extinction coefficient (km^{-1}) at mid-visible wavelengths zonally averaged from 40°S to 20°S at 18 km (panel a), 20 km (panel b), 22 km (panel c), and 24 km (panel d). Colored solid lines denote different emission scenarios "given in the key". The black carbon mass fraction is 2.5% in each scenario. The black dashed line denotes the control case without Australian smoke injection. Mid-visible aerosol extinction coefficients observed by SAGEIII-ISS are denoted by gray circles and the means are denoted by the magenta symbols.

of the model freely for 1 year (using model-generated meteorology). As such, the model does not capture the record-breaking NH polar vortex in 2020 (Lawrence et al., 2020), nor does it capture the QBO disruption that occurred in February 2020 (Saunders et al., 2020). We did not include material from the June 2019 Raikoke volcanic eruption at 48°N. Using this model configuration, we ran nine ensemble member pairs by perturbing the initial condition at the beginning of the free-running portion of the nominal simulation (i.e., 3xPNE and 2.5% BC fraction) starting on December 29, 2019.

3. Results

3.1. Plume Rise and Evolution

The smoke plume was observed to rise above 20 km in the first month (Kablick et al., 2020; Khaykin et al., 2020). As shown in Figure 1, the simulated stratospheric background aerosol extinction coefficient at mid-visible wavelengths is between 1×10^{-4} and 3×10^{-4} km^{-1} from 18 to 24 km without the Australian smoke. The background aerosol is mostly composed of pure sulfate from oxidation of carbonyl sulfide and mixed organic-sulfate particles of tropospheric origin (Froyd et al., 2009; Murphy et al., 2014; Yu et al., 2016). SAGE III/ISS shows that aerosol extinction coefficients in Southern Hemisphere (SH) midlatitudes are enhanced by a factor of 3–5 from 18 to 24 km in early 2020. In the simulations shown in Figure 1, the 3xPNE scenario agrees best with SAGE III/ISS. The simulation with 5xPNE overestimates the observed extinction coefficients by a factor of 3–10 above 20 km, while the simulation with 1xPNE shows negligible enhancement over background above 20 km. Our model further suggests that the injected smoke mass is large enough to enhance the global lower stratospheric aerosol mixing ratio by a factor of 1–3 by March of 2020 (Figure S1).

Black carbon absorbs sun light and the heating lofts the smoke plume and surrounding air parcels. The amount of heating, and therefore the rate of plume rise is determined by the amount of BC within the smoke. However, the total optical depth is dominated by the amount of OC in the plume. Thus, we use timing of the observed plume rise to constrain the amount of BC in the plume and the observed extinction

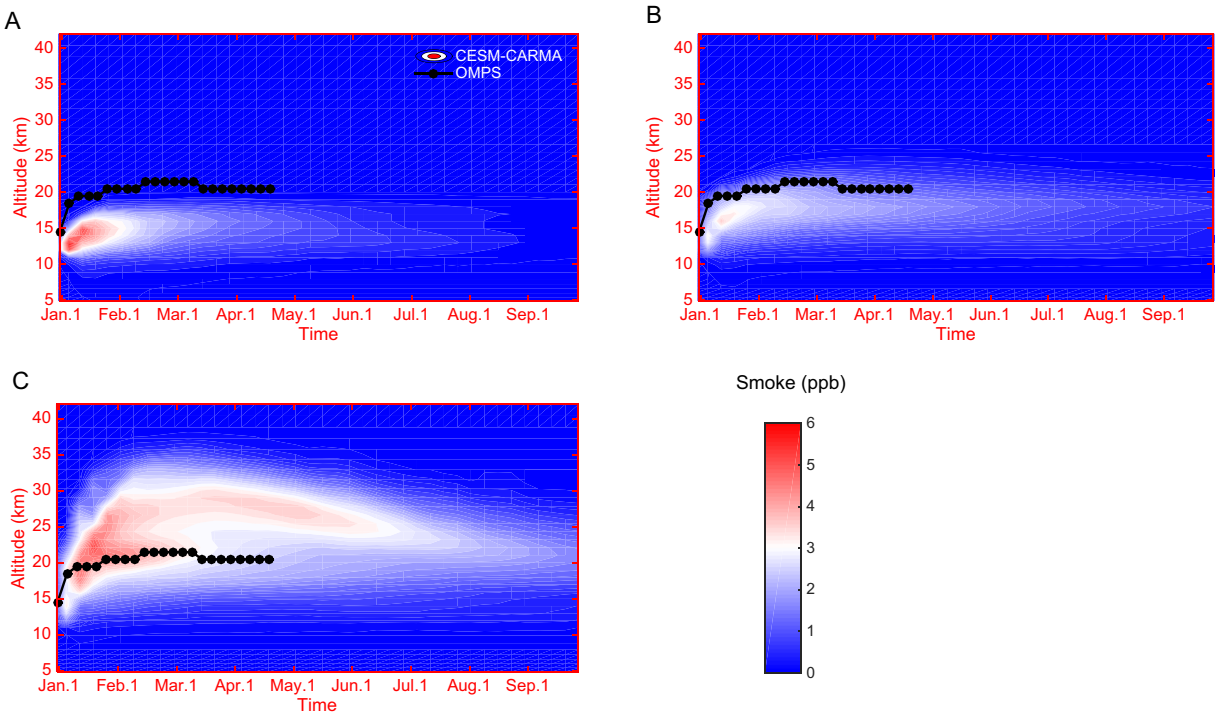

Figure 2. (a) Simulated smoke mass mixing ratio (unit: ppb) as a function of time averaged from 60°S to 20°S is shown in color contours. The smoke particles are assumed to be pure OC (without BC). Observed smoke maximum altitude by the OMPS satellite is shown in white circles. OMPS maximum altitude defined in this study is the highest altitude where the zonal mean aerosol extinction coefficient is greater than 5×10^{-4} km^{-1} at 675 nm; (b) same as (a), but with 2.5% BC in the smoke; (c) same as (a), but with 5% BC in the smoke. The total injected smoke mass in all panels is 0.9 Tg (i.e., 3xPNE). BC, black carbon; OC, organic carbon; OMPS, Ozone Mapping and Profiler Suite.

increases to constrain the total optical depth as shown in Figures 1 and 2. Figure 1 shows the sensitivity of the extinction to different smoke amounts using a BC fraction of 2.5%. The smoke in the 1xPNE simulation does not rise above 20 km and thus simulation compares poorly with the observations while the 5xPNE simulation greatly overestimates the observed extinction coefficients. The simulated smoke in the 3xPNE scenario with 2.5% BC agrees best with SAGE III/ISS observations.

The OMPS-LP data in Figure 2 show that the smoke plume rose from 16 to 22 km between 13 January and early March. Simulations with the same total injected smoke mass (i.e., 3xPNE) but with various BC mass fractions (0%, 2.5%, 5%) are shown in the panels of Figure 2. Consistent with the 2017 PNE (Yu et al., 2019) and 2013 California Rim fire (Yu et al., 2016), our simulations with 2.5% of BC in the smoke particles best match the observed plume rise (Figure 2b). Without BC in the simulation, the smoke failed to climb above 18 km (Figure 2a) while a smoke plume with 5% BC rose above 30 km in the first month (Figure 2c).

We calculated the Transformed Eulerian Mean residual vertical velocity ($\overline{w}^*$) (Andrews et al., 1987) from the 3xPNE 2.5% BC and baseline (no smoke) simulations to diagnose the mean meridional smoke-induced vertical air motion. These calculations indicate significant zonally averaged upward motion in the midlatitudes of the Southern Hemisphere in January when the smoke remained relatively concentrated (Figure S2). In later months, the stratospheric temperature adjustment balanced the radiative heating, and that combined with plume dilution resulted in no further significant vertical motion.

3.2. Smoke's Latitudinal Spread

OMPS-LP satellite observations (Figure S3) show that smoke particles spread through the entire SH stratosphere within 2 months. In the lower stratosphere (<16 km), transport was polewards reaching 80°S in February of 2020. Portions of the smoke that were lofted higher (up to 25 km) moved equatorwards. The higher

the smoke reached, the longer its residence time and the greater the mixing throughout the hemisphere due to wind shear and dispersion (Yu et al., 2019). Simulations suggest that a small amount of smoke was transported across the equator to the Northern Hemisphere (NH) in late January 2020. However, we don't have observational evidence for the cross-latitude transport because the NH stratosphere was heavily influenced by volcanic smoke in early 2020. Observations from Mauna Loa Observatory lidar (Figure S4) show that the aerosol backscatter ratio is a factor of 3–5 larger than model simulations. The large discrepancy is likely attributed to the Raikoke and Ulawun volcanic injections, which are not included in the model results presented in this study.

3.3. Persistent Stratospheric Warming

For the observational temperature analysis, we use the Modern Era Retrospective Analysis for Research and Applications-2 (MERRA-2) reanalysis (Gelaro et al., 2017) monthly mean assimilated (ASM) collection (GMAO et al., 2020) (see details of the MERRA-2 reanalysis in the Supporting Information Text S2). The MERRA-2 reanalysis residual temperature anomaly (with QBO, polar vortex and long-term trend removed) shows significant stratospheric warming starting from January of 2020 from 50°S to 50°N (Figure S5). Zonally averaged residual temperature anomalies as large as 1 K are found over half of the globe in the lower stratosphere in January of 2020. In Figure S6, the largest MERRA-2 residual anomalies in January and February are found in the lower stratospheric midlatitude SH and tropics. MERRA-2 warming decays significantly in March and April. Here we hypothesize that the stratospheric warming in the Southern Hemisphere (SH) and tropics is a consequence of smoke-induced diabatic heating.

We use CESM-CARMA to diagnose the spatial-temporal distribution and magnitude of the warming caused by the 2019–2020 ANY event. The magnitude and spatial pattern of the warming in the simulations are similar to the MERRA-2 residual temperature anomalies (Figure S6). We have completed 9-member ensembles of simulations both with and without the smoke, and all simulations with smoke find the consistent stratospheric warming as shown in Figure S7. Modeled warming persists from January to September of 2020, while the warming signals in MERRA-2 decay quickly in March. However, the actual temperature (as indicated by MERRA-2) will be impacted by factors not included in our model runs such as volcanic aerosols and internal variability. Shown in Figure 3a, the simulated smoke in the 3xPNE simulation warms the midlatitude stratosphere (60°S–20°S) by 1–2 K in February–March 2020, agreeing with the warming signals in the MERRA-2 reanalysis data. The simulation with 5xPNE, which includes more absorbing material, doubles the modeled temperature anomaly and does not match observations well. The shadings and error bars in Figure 3a denote the simulated variability (one standard deviation) in the ensemble runs. The smoke-induced temperature anomalies are greater than model variability (derived from ensemble runs), which indicates that the simulated stratospheric warming is statistically significant in both 3xPNE and 5xPNE simulations. On the other hand, the limited BC in the 1xPNE simulation did not produce any statistically robust stratospheric warming. The stratospheric warming is most significant in the midlatitudes of SH where the smoke entered the stratosphere. Weaker but still significant warming is predicted by simulations for mid-high latitudes in SH and tropics (Figures 3b–3d). Clearly, increasing the amount of BC leads to stronger stratospheric warming. Smoke in the 1xPNE scenario has no effect on air temperature at 26 mb (about 25 km in the tropics) (Figure 3b). In contrast, smoke in the 5xPNE simulation warms the stratospheric air at 26 hPa by 1–2 K. No significant temperature response was found for any emission scenario in the upper troposphere (~300 hPa) below where the smoke is located (Figure 3e). This contrasts with cases of volcanic eruptions (Agung, El Chichon and Pinatubo) that produce temperature decreases at 300 hPa, while heating the stratosphere at 50 hPa by as much as 1.5 K (Free & Angell, 2002).

The model reproduces the spatial distribution of the warming signals with warming in the upper tropospheric air of midlatitudes and lower stratosphere in the tropics (Figures S5–S6). The model produces more persistent warming than indicated by the MERRA-2 reanalysis data set in the lower stratosphere of SH and tropics. While it is possible that the radiative-dynamical feedback in the model could be overestimating the warming, it is worth noting that other recent stratospheric perturbations have likely influenced stratospheric temperatures, including the Raikoke and Ulawun volcanoes (Figure S4), not to mention other sources of stratospheric internal variability (e.g., QBO, polar vortex) that could obscure the persistent warming from

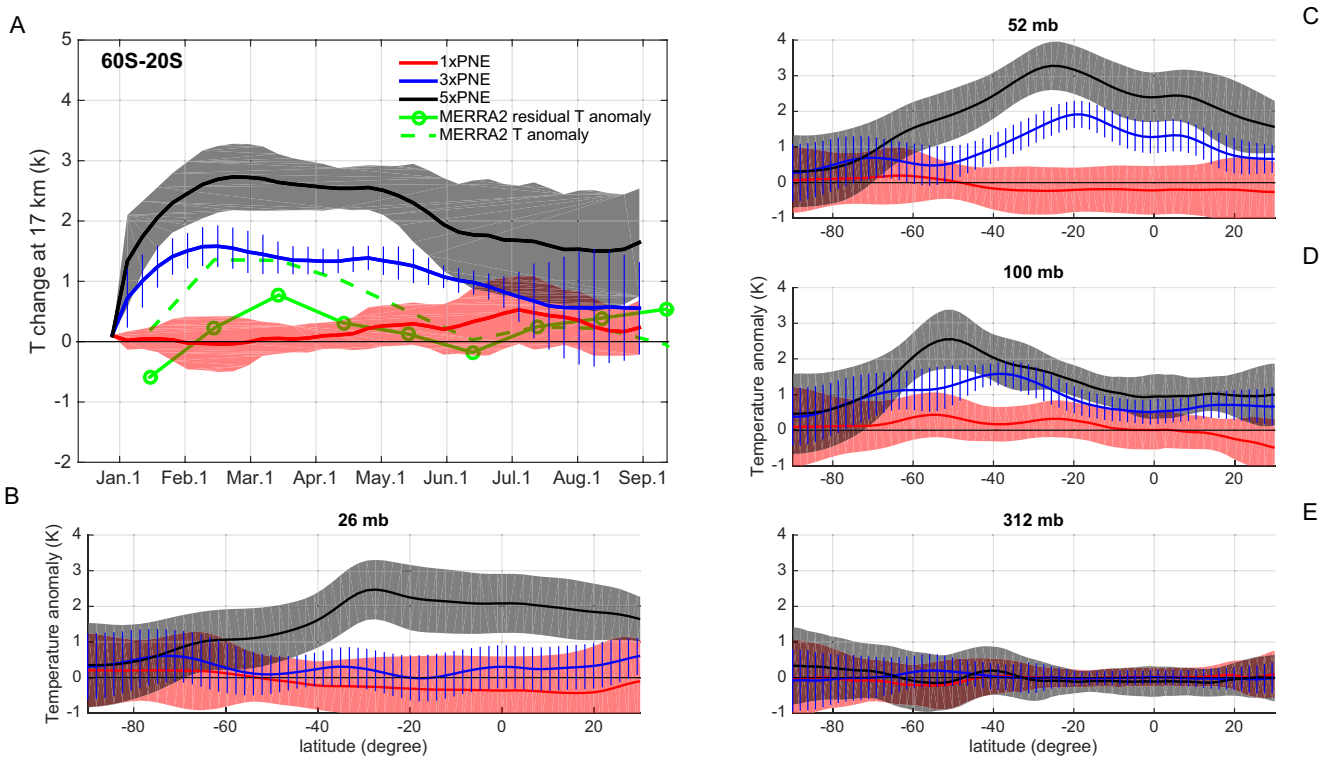

Figure 3. (a) Simulated temperature anomalies (unit: K) at 18 km averaged between 60°S and 20°S due to smoke from various emission scenarios (1xPNE, 3xPNE, and 5xPNE). The dashed green line represents the monthly MERRA2 anomalies at 18 km averaged from 60°S to 20°S. The solid green line with circles represents the monthly MERRA2 residual temperature anomalies at 18 km averaged from 60°S to 20°S, with QBO, polar vortex and long-term trend removed. (b) Simulated zonal mean temperature anomaly due to smoke at 26 mb averaged from February 1 to June 1, 2020. Different lines denote various emission scenarios. (c) Same as (b) but for anomalies at 52 mb; (d) same as (b) but for anomalies at 100 mb; (e) same as (b) but for anomalies at 312 mb. The shadings and error bars denote the simulated variability (one standard deviation) from ensemble runs.

the ANY fires. Also, while an attempt was made to remove the impacts of the QBO and NH polar vortex on temperature using multiple linear regression, this technique is limited in that it does not consider lags between the regressors and temperature, or nonlinear interactions.

3.4. Effective Radiative Forcing

Shown in Figure S8, our simulations with fixed sea surface temperature suggest that the peak local clear-sky effective radiative forcing (ERF) of the smoke is about −5 W m^{-2} at the top of the atmosphere (TOA) and the surface radiative forcing is about −20 W m^{-2} in eastern Australia averaged in the first 10 days since December 29, 2019. The simulated global mean clear-sky ERF is −0.03 W m^{-2} at TOA and the surface radiative forcing is −0.32 W m^{-2} averaged in year 2020. A small positive TOA forcing is estimated for 2017 PNE event (Christian et al., 2019) but note that they compute the instantaneous RF (IRF). For stratospheric BC, ERF is more climatically relevant since the fast adjustment from stratospheric warming causes a large longwave RF that opposes the shortwave RF from the BC absorption (Ban-Weiss et al., 2012). Thus, the IRF for stratospheric BC is positive while the ERF is negative. Also, the BC's effective radiative forcing at TOA is altitude dependent (Ban-Weiss et al., 2012) and the higher the smoke rise, the more negative forcing is expected at the TOA. The ERF at the TOA is estimated to decrease by ~0.02 W m^{-2} with the altitude the smoke rises to from 20 to 30 km.

3.5. Change in Stratospheric Ozone at Middle and High Latitudes

In the 2017 PNE, local ozone minima associated with smoke in the first month were observed by satellite. Simulations showed that the ozone minima were mostly due to the displacement of ozone rich stratospher-

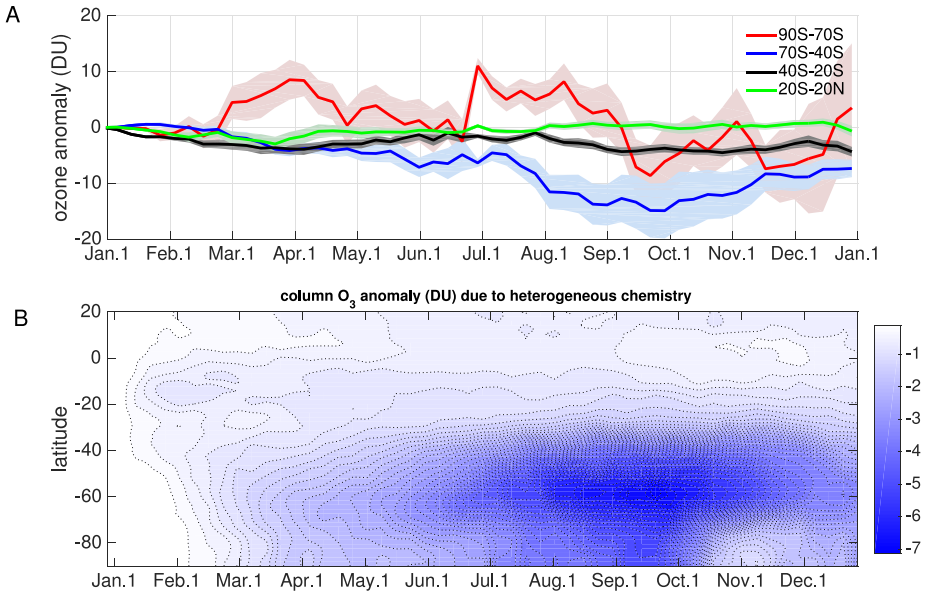

Figure 4. (a) Simulated change of the column ozone (DU) averaged in different latitude bands due to ANY smoke. Shadings denote one standard deviation of the 15 ensemble simulations w/and w/o the smoke. Winds and temperature fields in the simulations are self-generated in the model (i.e., free running). We assume organics provide a surface reaction area similar as sulfuric acid at the same temperature. (b) Simulated change of column ozone (DU) due to the heterogeneous chemistry on the smoke particles only. ANY, Australian New Year.

ic air by ozone-poor tropospheric air when the plume rose (Yu et al., 2019). Khaykin et al. (2020) reported similar ozone minima within the individual smoke plume for the 2019–2020 ANY event. The ozone minima vanished into the background when the fire plume stopped rising. However, in addition to the in-plume ozone minima, simulations for the 2019–2020 ANY event predict persistent ozone negative anomalies in SH middle-high latitudes from August to December of 2020 (Figure 4). We conducted sensitivity simulations to investigate the causes of the modeled ozone loss due to the 2019–2020 ANY smoke.

Volcanic sulfuric acid particles (such as those from Pinatubo) provide effective reaction surfaces for heterogeneous chemical reactions that deplete ozone (Solomon et al., 1999). It is not clear if aged organic particles (which are likely coated or mixed with sulfuric acid within a few months in the stratosphere) provide as effective surface areas for heterogeneous chemistry as does sulfuric acid aerosol. In the simulation in Figure 4 we assume that smoke particles provide a surface reaction rate equal to that of sulfuric acid particles, which we assume is an upper bound for our estimate on the chemistry-induced ozone depletion from the smoke. Shown in Figure 4a, comparison between simulations with and without the smoke shows that the ANY smoke causes persistent ozone negative anomalies of 10–20 Dobson units (DU) in SH middle and high latitudes (40°S–90°S). Heterogeneous chemistry on the ANY smoke particles causes ozone negative anomalies of 5–7 DU in the latitude band of 40°S–90°S (Figure 4b). Shown in Figure S9, we have also conducted sensitivity simulations in which the winds and temperature are driven by the GEOS-5 analysis. Similar ozone depletion is predicted when comparing simulations with the heterogeneous chemistry turned on and off in the model. The rest of the simulated ozone anomalies are due to heating and dynamical changes induced by the ANY smoke. This smoke-induced depletion modestly enhances the depth of the ozone hole in our simulations. Because the simulated smoke particles remain mostly in midlatitudes, the predicted ozone anomalies are larger along the vortex edge than in the core of the vortex. The simulated Antarctic ozone hole size (defined as the area with total column ozone less than 220 DU) averaged from 7 September to 13 October of 2020 is about 2.1×10^7 km^2 with ANY smoke, which is about 12% larger than the no smoke case (Figure S10). This simulated enhancement in ozone hole area due to smoke is consistent with the observed 2020 ozone hole, which was the third largest in the past decade and 18% larger than the 2010–2019 average. Further work is needed to assess the dynamical impacts of the ANY smoke on the SH circulation in 2020.

4. Summary

From December 29, 2019 to January 4, 2020, Australian wildfires injected about 0.9 Tg of smoke into the stratosphere, about three times more than the 2017 Pacific Northwest event injected. This Australian event is the largest stratospheric smoke injection observed by satellites to date. Satellite observations show that the smoke spread over the entire Southern Hemisphere (SH) and the large-scale smoke (not individual plumes) climbed to 22 km in the first 3 months. By comparing the simulated plume rise with observations, we estimate the smoke particles were composed of 2.5% of black carbon and 97.5% of organic carbon or other materials by mass. The 2.5% mass fraction of black carbon is similar to the values derived from the 2017 PNE stratospheric smoke in British Columbia and Washington State (Yu et al., 2019) and from the 2016 tropospheric smoke from the Rim fire in California (Yu et al., 2016). Numerical simulations predict that the Australian smoke will produce detectable levels of visible light extinction in the stratosphere for over one year.

In model simulations, the midlatitude stratosphere in the Southern Hemisphere was warmed by 1–2 K for 6 months from the diabatic heating of black smoke particles. Similar stratospheric warming is found in MERRA2 reanalysis data set for January through March as well, although the modeled warming is more persistent than that in the MERRA2 analysis. The simulated warming also extends to the midlatitudes of the NH, which is due to downward transport of air in the NH in response to the smoke's heating. However, the model did not include volcanic eruptions that occurred in the tropics and NH in 2019 and likely perturbed the stratosphere in the NH. The model predicts a global mean clear-sky effective radiative forcing of -0.03 W m^{-2} at TOA and a global surface radiative forcing of -0.32 W m^{-2} averaged in 2020. When treated chemically the same as sulfate aerosol, the 2019–2020 Australian smoke particles are predicted to cause ozone loss of about 10–20 DU in the SH mid-high latitudes. Our study highlights that record-breaking wildfire smoke can cause persistent impacts to stratospheric dynamics and chemistry.

Data Availability Statement

MERRA2 data are available at https://gmao.gsfc.nasa.gov/reanalysis/MERRA-2/; Model simulations are available at https://osf.io/g2j63/?view_only=9f4b610660a4437ca1b4617244c6caf8; SAGEIII-ISS data are available at https://eosweb.larc.nasa.gov/project/sageiii-iss/g3bssp_v5_1; OMPS_LP data are available at https://ozoneaq.gsfc.nasa.gov/data/omps/ QBO EOFs used in the regression fit are from https://acd-ext.gsfc.nasa.gov/Data_services/met/qbo/qbo.html

Acknowledgments
This study was supported by the second Tibetan Plateau Scientific Expedition and Research Program (2019QZKK0604), Guangdong Innovative and Entrepreneurial Research Team Program (2016ZT06N263), and National Science Foundation of China (41805094). Owen B. Toon was supported by the University of Colorado and the Open Philanthropy Foundation. The CESM project is supported by the National Science Foundation and the Office of Science (BER) of the US Department of Energy. The authors acknowledge high-performance computing support from Cheyenne (https://doi.org/10.5065/D6RX99HX) provided by NCAR's Computational and Information Systems Laboratory, sponsored by the National Science Foundation. This work also used the RMACC Summit supercomputer, which was supported by the National Science Foundation (awards ACI-1532235 and ACI-1532236), the University of Colorado Boulder, and Colorado State University.

References

Andreae, M. O. (2019). Emission of trace gases and aerosols from biomass burning—An updated assessment. *Atmospheric Chemistry and Physics*, *19*, 8523–8546. https://doi.org/10.5194/acp-19-8523-2019

Andrews, D. G., Holton, J. R., & Leovy, C. B. (1987). Middle atmosphere dynamics (Vol. xi, p. 489). Orlando: Academic Press.

Ban-Weiss, G. A., Cao, L., Bala, G., & Caldeira, K. (2012). Dependence of climate forcing and response on the altitude of black carbon aerosols. *Climate Dynamics*, *38*, 897–911. https://doi.org/10.1007/s00382-011-1052-y

Bardeen, C. G., Toon, O. B., Jensen, E. J., Marsh, D. R., & Harvey, V. L. (2008). Numerical simulations of the three-dimensional distribution of meteoric dust in the mesosphere and upper stratosphere. *Journal of Geophysical Research*, *113*(D17). https://doi.org/10.1029/2007jd009515

Christian, K., Wang, J., Ge, C., Peterson, D., Hyer, E., Yorks, J., & McGill, M. (2019). Radiative forcing and stratospheric warming of pyrocumulonimbus smoke aerosols: First modeling results with multisensor (EPIC, CALIPSO, and CATS) views from space. *Geophysical Research Letters*, *46*, 10061–10071. https://doi.org/10.1029/2019GL082360

de Laat, A. T. J., Zweers, D. C. S., Boers, R., & Tuinder, O. N. E. (2012). A solar escalator: Observational evidence of the self-lifting of smoke and aerosols by absorption of solar radiation in the February 2009 Australian Black Saturday plume. *Journal of Geophysical Research*, *117*, D04204. https://doi.org/10.1029/2011jd017016

Forrister, H., Liu, J., Scheuer, E., Dibb, J., Ziemba, L., Thornhill, K. L., et al. (2015). Evolution of brown carbon in wildfire plumes. *Geophysical Research Letters*, *42*, 4623–4630. https://doi.org/10.1002/2015GL063897

Free, M., & Angell, J. K. (2002). Effect of volcanoes on the vertical temperature profile in radiosonde data. *Journal of Geophysical Research*, *107*(D10), 16. https://doi.org/10.1029/2001JD001128

Fromm, M., Lindsey, D. T., Servranckx, R., Yue, G., Trickl, T., Sica, R., et al. (2010). The untold story of pyrocumulonimbus. *Bulletin of the American Meteorological Society*, *91*, 1193–1210. https://doi.org/10.1175/2010bams3004.1

Froyd, K. D., Murphy, D. M., Sanford, T. J., Thomson, D. S., Wilson, J. C., Pfister, L., & Lait, L. (2009). Aerosol composition of the tropical upper troposphere. *Atmospheric Chemistry and Physics*, *9*(13), 4363–4385. https://doi.org/10.5194/acp-9-4363-2009

Gelaro, R., McCarty, W., Suárez, M. J., Todling, R., Molod, A., Takacs, L., et al. (2017). The Modern-Era Retrospective Analysis for Research and Applications, Version 2 (MERRA-2). *Journal of Climate*, *30*(14), 5419–5454. https://doi.org/10.1175/jcli-d-16-0758.1

Global Modeling and Assimilation Office (GMAO). (2020). *MERRA-2 instM_3d_asm_Np: 3d, monthly mean, instantaneous, pressure-level, assimilation, assimilated meteorological fields V5.12.4*. Greenbelt, MD: Goddard Earth Sciences Data and Information Services Center (GES DISC). https://doi.org/10.5067/2E096JV59PK7

Kablick, G. P., Allen, D. R., Fromm, M. D., & Nedoluha, G. E. (2020). Australian pyroCb smoke generates synoptic-scale stratospheric anticyclones. *Geophysical Research Letters*, *47*, e2020GL088101. https://doi.org/10.1029/2020gl088101

Khaykin, S., Legras, B., Bucci, S., Sellitto, P., Isaksen, L., Tense, F., et al. (2020). The 2019/20 Australian wildfires generated a persistent smoke-charged vortex rising up to 35 km altitude. *Communications Earth & Environment*, *1*, 22. https://doi.org/10.1038/s43247-020-00022-5

Khaykin, S. M., Godin-Beekmann, S., Hauchecorne, A., Pelon, J., Ravetta, F., & Keckhut, P. (2018). Stratospheric smoke with unprecedentedly high backscatter observed by lidars above southern France. *Geophysical Research Letters*, *45*, 1639–1646. https://doi.org/10.1002/2017gl076763

Lawrence, Z. D., Perlwitz, J., Butler, A. H., Manney, G. L., Newman, P. A., Lee, S. H., & Nash, E. R. (2020). The remarkably strong Arctic stratospheric polar vortex of winter 2020: Links to record-breaking Arctic Oscillation and ozone loss. *Journal of Geophysical Research: Atmospheres*, *125*, e2020JD033271. https://doi.org/10.1029/2020jd033271

Malone, R. C., Auer, L. H., Glatzmaier, G. A., Wood, M. C., & Toon, O. B. (1985). Influence of solar heating and precipitation scavenging on the simulated lifetime of post-nuclear war smoke. *Science*, *230*, 317–319.

Mills, M. J., Toon, O. B., Turco, R. P., Kinnison, D. E., & Garcia, R. R. (2008). Massive global ozone loss predicted following regional nuclear conflict. *Proceedings of the National Academy of Sciences of the United States of America*, *105*(14), 5307–5312. https://doi.org/10.1073/pnas.0710058105

Murphy, D. M., Froyd, K. D., Schwarz, J. P., & Wilson, J. C. (2014). Observations of the chemical composition of stratospheric aerosol particles. *Quarterly Journal of the Royal Meteorological Society*, *140*, 1269–1278. https://doi.org/10.1002/qj.2213

Peterson, D. A., Campbell, J. R., Hyer, E. J., Fromm, M. D., Kablick, G. P., Cossuth, J. H., & DeLand, M. T. (2018). Wildfire-driven thunderstorms cause a volcano-like stratospheric injection of smoke. *npj Climate and Atmospheric Science*, *1*, 1. https://doi.org/10.1038/s41612-018-0039-3

Peterson, D. A., Hyer, E., Campbell, J., Fromm, M., Bennese, C., Berman, M., & Van, T. (2020). *Quantifying the impact of intense pyroconvection on stratospheric aerosol loading*. Retrieved from https://ams.confex.com/ams/2020Annual/videogateway.cgi/id/521800?recordingid=521800

Robock, A. (1988). Enhancement of surface cooling due to forest fire smoke. *Science*, *242*, 4880. https://doi.org/10.1126/science.242.4880.911

Saunders, M. A., Adam, A. S. R., & Smallwood, J. R. (2020). The quasi-biennial oscillation: A second disruption in four years. *Earth and Space Science Open Archive*. https://doi.org/10.1002/essoar.10504326.1

Solomon, S. (1999). Stratospheric ozone depletion: A review of concepts and history. *Reviews of Geophysics*, *37*(3), 275–316. https://doi.org/10.1029/1999RG900008

Toon, O. B., Bardeen, C. G., Robock, A., Xia, L., Kristensen, H., McKinzie, M., et al. (2019). Rapidly expanding nuclear arsenals in Pakistan and India portend regional and global catastrophe. *Science Advances*, *5*(10). https://doi.org/10.1126/sciadv.aay5478

Toon, O. B., Turco, R. P., Westphal, D., Malone, R., & Liu, M. (1988). A multidimensional model for aerosols—Description of computational analogs. *Journal of the Atmospheric Sciences*, *45*(15). https://doi.org/10.1175/1520-046910.1175/1520-0469(1988)045<2123:ammfad>2.0.co;2

Torres, O., Bhartia, P. K., Taha, G., Jethva, H., Das, S., Colarco, P., et al. (2020). Stratospheric injection of massive smoke plume from Canadian boreal fires in 2017 as seen by DSCOVR-EPIC, CALIOP, and OMPS-LP observations. *Journal of Geophysical Research: Atmospheres*, *125*, e2020JD032579. https://doi.org/10.1029/2020jd032579

Yu, P., Murphy, D. M., Portmann, R. W., Toon, O. B., Froyd, K. D., Rollins, A. W., et al. (2016). Radiative forcing from anthropogenic sulfur and organic emissions reaching the stratosphere. *Geophysical Research Letters*, *43*, 9361–9367. https://doi.org/10.1002/2016gl070153

Yu, P., Toon, O. B., Bardeen, C. G., Mills, M. J., Fan, T., English, J. M., & Neely, R. R. (2015). Evaluations of tropospheric aerosol properties simulated by the Community Earth System Model with a sectional aerosol microphysics scheme. *Journal of Advances in Modeling Earth Systems*, *7*, 865–914. https://doi.org/10.1002/2014ms000421

Yu, P., Toon, O. B., Bardeen, C. G., Zhu, Y., Rosenlof, K. H., Portmann, R. W., et al. (2019). Black carbon lofts wildfire smoke high into the stratosphere to form a persistent plume. *Science*, *365*, 587–590. https://doi.org/10.1126/science.aax1748

References From The Supporting Information

Iacono, M. J., Delamere, J. S., Mlawer, E. J., Shephard, M. W., Clough, S. A., & Collins, W. D. (2008). Radiative forcing by long-lived greenhouse gases: Calculations with the AER radiative transfer models. *Journal of Geophysical Research*, *113*, D13103. https://doi.org/10.1029/2008JD009944.Kablick.et.al

Mackowski, D. W., & Mishchenko, M. I. (2011). A multiple sphere T-matrix Fortran code for use on parallel computer clusters. *Journal of Quantitative Spectroscopy and Radiative Transfer*, *112*, 2182–2192. https://doi.org/10.1016/j.jqsrt.2011.02.019

Wallace, J. M., Panetta, R. L., & Estberg, J. (1993). Representation of the equatorial stratospheric quasi-biennial oscillation in EOF phase space. *Journal of the Atmospheric Sciences*, *50*, 1751–1762. https://doi.org/10.1175/1520-0469(1993)050<1751:rotesq>2.0.co;2